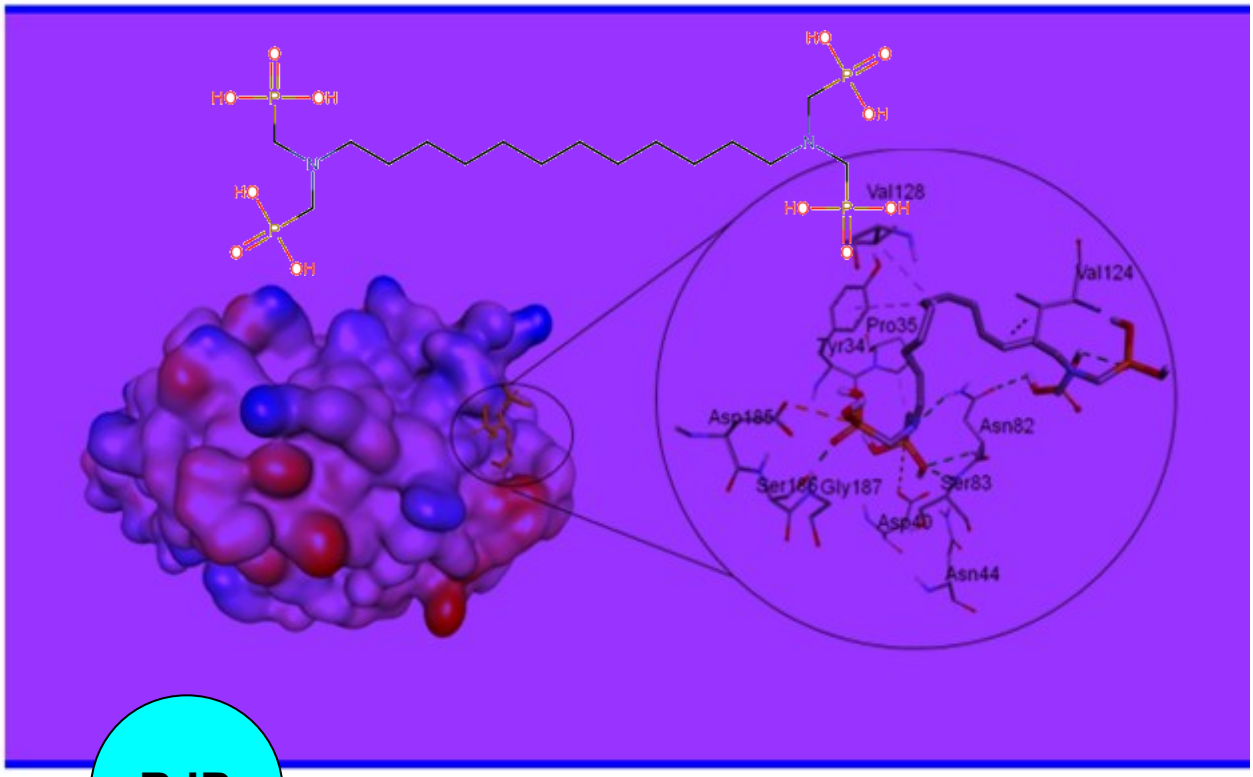

BJP

Bangladesh Journal of Pharmacology

Research Article

Synthesis, characterization, and antibacterial activity of a novel hybrid material layered double hydroxide doped by diaminododecylphosphonic acid

A Journal of the Bangladesh Pharmacological Society (BDPS)
Journal homepage: www.bdpsjournal.org; www.banglajol.info
Abstracted/indexed in Academic Search Complete, Agroforestry Abstracts, Asia Journals Online, Bangladesh Journals Online, Biological Abstracts, BIOSIS Previews, CAB Abstracts, Current Abstracts, Directory of Open Access Journals, EMBASE/Excerpta Medica, Global Health, Google Scholar, HINARI (WHO), International Pharmaceutical Abstracts, Open J-gate, Science Citation Index Expanded, SCOPUS and Social Sciences Citation Index
Bangladesh J Pharmacol 2024; 19: 135-146
ISSN: 1991-0088

Synthesis, characterization, and antibacterial activity of a novel hybrid material layered double hydroxide doped by diaminododecylphosphonic acid

Djamila Ikhou[1],Farouk Boudou[2], Hanane Ziani[1], M'Hamed Kaid[1] and Didier Villemein[3]

[1]Laboratory of Physico-chemical Studies, Department of Chemistry, Faculty of Sciences, University of Saida, Dr Moulay Tahar, 20000, Algeria; [2]Department of Biology, Faculty of Natural and Life Sciences, Djillali Liabes University of Sidi-Bel-Abbes, Sidi-Bel-Abbes 22000, Algeria; [3]EnsiCaen, LCMT, UMR CNRS 6507, INC3M,FR 338,Université de Caen, Caen, France, 14050, France.

Article Info

Received: 2 February 2025
Accepted: 24 February 2025
Available Online: 25 February 2025
DOI: 10.3329/bjp.v19i4.79648

Cite this article:
Ikhou D, Boudou F, Ziani H, Kaid M, Villemein D. Synthesis, characterization, and antibacterial activity of a novel hybrid material layered double hydroxide doped by diaminododecylphosphonic acid. Bangladesh J Pharmacol. 2024; 19: 135-46.

Abstract

A novel hybrid material Zn/Al-diaminododecylphosphonic acid (DADPHA) layered double hydroxide (LDH) was synthesized and characterized for its structural, electronic, and antibacterial properties. X-ray diffraction confirmed DADPHA intercalation, increasing basal spacing from 7.55 to 7.95 angstrom. The crystallite size of Zn/Al-DADPHA (11.10 nm) was smaller than that of Zn/Al-SO_4 LDH (16.70 nm), indicating modification. FTIR confirmed phosphonic acid functional groups, while SEM revealed a morphological shift from hexagonal platelets to aggregated structures. Zn/Al-DADPHA exhibited significant antibacterial activity, with inhibition zones of 25.6 mm (*Escherichia coli*), 10.9 mm (*Pseudomonas aeruginosa*), 30.2 mm (*Staphylococcus aureus*), and 25.5 mm (*Bacillus cereus*). Molecular docking revealed strong ligand-protein interactions (-7.1 to -9.4 kcal/mol). DFT calculations showed a HOMO-LUMO gap of 4.82 eV, confirming electronic stability. MD simulations over 100 ns indicated complex stability with RMSD below 2.5 angstrom. These findings highlight the potential of Zn/Al-DADPHA LDH for biomedical and antimicrobial applications.

Introduction

Layered double hydroxides (LDHs), also known as anionic clays, are formed by the non-covalent stacking of lamellar sheets (Sharma et al., 2023). These structures are made up of basic two-dimensional solids produced by stacking brucite-like layers, $Mg(OH)_2$, which gain a positive charge as a result of trivalent cations like M(III) partially replacing divalent cations M(II) (Theiss et al., 2016). This positive charge is balanced by interlamellar anions present or intercalated within the interlayer space of the metal hydroxide sheets (Wang et al., 2023).

The general formula for LDHs is given by:

$$[M^{2+}_{1-x}M^{3+}_{x}\,(OH)_2]^{x+}[A^{n-}{}_{x/y}\cdot yH_2O]^{x-}$$

where M^{2+} and M^{3+} represent divalent and trivalent cations, respectively; A^{n-} is the intercalated anion; x is the charge density, defined as $x = M^{3+}/(M^{2+} + M^{3+})$; and y is the number of water molecules in the interlayer space (Chen et al., 2022).

To achieve a pure hydrotalcite phase, the stoichiometry must range between $0.2 < x < 0.33$, corresponding to a molar ratio M(II)/M(III) of 2 to 4. This allows the synthesis of various LDHs with different M^{2+}/M^{3+} ratios, including those with multiple metal cations. Intercalated anions are crucial for material function-

ality, particularly when organic anions are introduced into the interlayer space (Obalova et al., 2009). By altering their structural and morphological characteristics, several techniques are employed to maximize LDH performance, including co-precipitation (Wei et al., 2022), anion exchange (Jiang et al., 2022), and reconstruction (Cao et al., 2022). The most popular technique, co-precipitation, involves adding a basic solution in precise amounts to a solution of nitrate or chloride salts to precipitate metal cations simultaneously.

Due to their unique morphologies and structural characteristics, LDHs have found extensive applications in various catalytic domains (Si et al., 2021), including aldol condensation (Dubnova et al., 2022), Knoevenagel condensation (Stamate et al., 2023), Claisen-Schmidt condensation (Zavoianu et al., 2022), and polymerization (Mallakpour et al., 2021). They are also utilized in environmental applications for pollutant retention (Nava-Andrade et al., 2021), and in the pharmaceutical and biomedical fields. These hybrid materials have garnered significant interest due to their low toxicity and advanced biocompatibility (Shirin et al., 2021). The potential of double-layered hydroxide nanohybrids as effective anti-cancer drug carriers is highlighted by demonstrating their increased therapeutic efficacy in combination cancer therapies. This underscores the versatility of LDHs in biomedical applications, particularly in drug delivery systems designed to improve treatment outcomes (Kim et al., 2014). LDHs successfully intercalated the antibiotic into its interlayer space using the anion exchange method, demonstrating significant antibacterial activity against both Gram-positive and Gram-negative bacteria (Soleymani et al., 2024).

Aminophosphonic acids are highly regarded among functionalized acids because of their unique structure, which includes both amino and phosphonic acid groups (Rashad et al., 2021). These compounds are analogs of amino acids, where the carboxyl group is replaced by a phosphonic acid, P(O)(OH)2, or a phosphonic acid, P(O)(OH)R (Arribat et al., 2020). They demonstrate diverse biological activities, such as acting as antibacterial agents, enzyme inhibitors, catalytic antibody haptens, and anti-HIV agents (Kaboudin et al., 2022). The antibacterial action of silver nanoparticles incorporated in Zn-Al double-layered hydroxide is reported against *Escherichia coli* and *Staphylococcus aureus* due to the presence of hydroxide (–OH) groups and the nature of the metal cations, with Zn^{2+} being one of the most active due to its strong oligodynamic characteristics (Mishra et al., 2013). Additionally, Zn ions possess excellent antibacterial capacity and have been widely used as inorganic antibacterial agents (Saidin et al., 2021). The antibacterial activity of silver nanoparticles incorporated into Zn-Al layered double hydroxides has been demonstrated against *E. coli* and *S. aureus*. This effect is attributed to the presence of hydroxide (–OH) groups and the properties of metal cations, particularly Zn^{2+}, which exhibits strong oligodynamic characteristics (Mishra et al., 2013). Furthermore, Zn ions are known for their exceptional antibacterial properties and are widely utilized as inorganic antibacterial agents (Saidin et al., 2021). Furthermore, numerous hybrid organic-inorganic materials have been tested and continue to find applications in biomedical science (Liu et al., 2021).

In this study, a LDH (Zn/Al-SO_4) was synthesized by the co-precipitation method and intercalated using diaminododecylphosphonic acid (DADPHA), a chelating agent synthesized in this laboratory, to produce a novel hybrid material (Zn-Al/DADPHA) LDH. The synthesized materials were thoroughly characterized using spectroscopic techniques (FTIR, SEM and XRD). Their biological potential was evaluated through *in vitro* and *in silico* antibacterial assessments, demonstrating their efficacy as antibacterial inhibitors. This work highlights the versatility of LDHs in biomedical applications, particularly in the development of advanced antibacterial agents.

Materials and Methods

Chemicals and reagents

The materials synthesized for this study include diaminododecylphosphonic acid (DADPHA), prepared under microwave conditions (Ouazene et al., 2016), as well as Zn/Al-SO4 LDH and Zn/Al-DADPHA-LDH, both synthesized in the laboratory (Kadari et al., 2016). All chemicals and reagents, including solvents and microbiological culture media, were of analytical grade and used without further purification. These were procured from Sigma-Aldrich and Riedel-de Haen. All solutions were prepared using deionized water to ensure consistency and purity in the experimental procedures.

Synthesis of Zn/Al-LDH

LDH (Zn/Al-SO4) was synthesized using a co-precipitation method (Miyata, 1975), with a Zn/Al molar ratio of 3. Briefly, 150 mL of an aqueous solution containing metallic sulfates- 0.9M ZnSO4 and 0.3 M Al2 (SO4)3 - was added dropwise to a reactor containing 100 mL of distilled water. Simultaneously, a 1.5 M NaOH solution was introduced into the reactor while carefully maintaining the pH between 9 and 10. The reaction mixture was stirred continuously at room temperature for 24 hours. The resulting precipitate was filtered, washed repeatedly with distilled water, dried at 70°C, and ground to obtain the final Zn/Al-LDH material.

Synthesis of DADPHA

DADPHA was synthesized under microwave

irradiation. A mixture of phosphorous acid (40 mmol, 3.3 g), water (3 mL), and hydrochloric acid (3 mL) was added to 4.4 g of diaminododecane (20 mmol) in a quartz tube. The mixture was irradiated at 240 W for 2 min, followed by the rapid addition of 6.3 mL of formaldehyde (40 mmol). The reaction was further irradiated at 240 W for 30 min. The resulting product was filtered, washed with acetone, and rinsed with water to obtain pure DADPHA.

Synthesis of Zn-Al-DADPHA hybrid material

The Zn/Al-SO_4 LDH was modified by grafting with DADPHA to produce a novel hybrid material. Specifically, 20 g of Zn/Al-SO4 LDH was mixed with 100 mL of distilled water, while 1 g of DADPHA was dissolved in 50 mL of distilled water (ratio 1:20). The two solutions were combined and stirred for 24 hours. The resulting mixture was centrifuged, washed with deionized water and acetone, and dried at room temperature for 48 hours to yield the final Zn-Al-DADPHA hybrid material.

Characterization methods

The crystal phase composition and crystallite size of the materials were determined using a PANalytical X'PERT Pro diffractometer with Cu-Kα radiation (λ = 1.5406 angstrom), collecting data in the 2θ range of 5° to 60°. FTIR spectra were recorded using a PerkinElmer 16 PC spectrometer equipped with a temperature control unit (25.0 ± 0.1°C), with spectra acquired in the range of 4000 –400 cm^{-1}. The morphology and microstructure of the samples were analyzed using a high-resolution JEOL-JSM-F100 microscope (JEOL Ltd., Japan). The dislocation density (δ), which represents the number of defects and vacancies in the crystal material, was calculated based on the crystallite size. It was determined using the formula $\delta = 1/D^2$, where D is the crystallite size.

Antibacterial activity assessment

The antibacterial and antifungal efficacy of the synthesized compound, DADPA, was evaluated against selected bacterial strains, specifically *E. coli*, *Pseudomonas aeruginosa*, *S. aureus*, and *Bacillus cereus*. Bacterial cultures were incubated for 24 hours and then diluted in sterile saline to an approximate concentration of 10^8 CFU/mL, following the 0.5 McFarland standard. Sterile Mueller-Hinton agar plates were prepared with 20 mL of medium containing 2% beef extract, 17.5% acid hydrolysate of casein, 1.5% starch, and 1.5% agar. After inoculating the agar surface with a sterile swab dipped in the bacterial suspension, the plates were allowed to dry. Wells, 6.0 mm in diameter, were created on the agar surface and filled with the synthesized compound. All plates were incubated at 37°C for 24 hours, after which inhibition zones were measured with a caliper.

Selection of target protein and molecular docking

Molecular docking was performed to evaluate the binding affinity and interactions of the synthesized ligand (DADPHA) with four bacterial target proteins: *E. coli* PBP3 transpeptidase domain (PDB ID: 7ONN), *P. aeruginosa* genomics APC5556 (PDB ID: 1YOC), the N-terminal domain of *S. aureus* Fatty Acid Kinase A (FakA) (PDB ID: 7RM7), and *B. cereus* phospholipase C (PDB ID: 1AH7). The protein structures were obtained from the RCSB Protein Data Bank (www.rcsb.org) and prepared for docking studies. To ensure accurate binding site coverage, docking grid box parameters were optimized for each protein. Ligands were retrieved from PubChem and underwent energy minimization using the UFF force field with the conjugate gradients algorithm, which involved 200 optimization steps and a convergence criterion of an energy difference of 0.1 kcal/mol. Molecular docking simulations were carried out using PyRx-Python 0.8 with an exhaustiveness parameter of 8 to ensure a comprehensive exploration of binding poses. The docking results were analyzed using BIOVIA discovery studio visualizer to examine key protein-ligand interactions, including hydrogen bonds, hydrophobic interactions, and electrostatic contacts between ligands and amino acid residues in the target proteins. The binding affinity of each ligand to the target proteins was quantified using docking scores and free energy of binding.

Quantum chemical analysis of DADPHA

The quantum chemical properties of the synthesized ligand DADPHA were analyzed using density functional theory. Calculations were performed at the B3LYP/6-31G* level of theory, using the Gaussian 09W software package for all computational work. The molecular structures of all ligands were optimized to their lowest energy conformation. For visualization and orbital analysis, GaussView was employed to render the molecular structures and the spatial distribution of the frontier molecular orbitals. Key electronic properties, including the energies of the highest occupied molecular orbital (HOMO) and the lowest unoccupied molecular orbital (LUMO), were calculated based on the optimized structures. The HOMO-LUMO energy gap (Eg) was determined as the energy difference between these orbitals, providing insights into the ligand's electronic stability and reactivity. The HOMO and LUMO orbitals were visualized to highlight electron-rich and electron-deficient areas that may play critical roles in their chemical interactions and potential binding to target proteins.

Molecular dynamics simulations

To further validate the docking results and assess the dynamic stability of ligand-protein interactions, molecular dynamics (MD) simulations were performed. These simulations were conducted using the GROMACS 2023-GPU package with the CHARMM36m force field to provide a realistic representation of

biomolecular behavior in a dynamic environment. Each selected complex was solvated in a triclinic box using the TIP3P water model and neutralized by adding Na^+ and Cl^- ions to achieve a physiological salt concentration of 150 mM. Prior to the production run, energy minimization was carried out to resolve steric clashes and optimize system geometry. Equilibration was then performed in two phases: an NVT ensemble (constant volume and temperature) and an NPT ensemble (constant pressure and temperature), each for 2 nsec, ensuring system stability before the simulation phase. The production MD simulations were executed for 100 nsec at a constant temperature of 300 K and a pressure of 1 bar. Post-simulation trajectory analysis was conducted to evaluate global protein dynamics, backbone flexibility, and the stability of protein-ligand interactions over time. Key structural parameters were analyzed to evaluate the stability and dynamics of the protein-ligand complexes throughout the simulation period. The Root Mean Square Deviation (RMSD) was calculated to assess the structural stability and conformational changes of the complexes over time. To investigate the local flexibility of individual residues, Root Mean Square Fluctuation (RMSF) analysis was performed, providing insights into residue-specific mobility. Additionally, the Radius of Gyration (Rg) was measured to determine the overall compactness and structural folding of the protein-ligand complexes, offering a quantitative measure of their global stability.

Results

FT-IR spectroscopic analysis of Zn/Al-SO_4 LDH and Zn/Al-DADPHA

The FT-IR spectra of Zn/Al-SO4-LDH and Zn/Al-DADPHA are shown in Figure 1A. The spectral analysis provides insight into the structural and compositional differences between the two materials, particularly in terms of their hydroxyl groups, sulfate vibrations, and the incorporation of DADPHA. The broad and intense bands observed in the region between 3400 cm^{-1} and 3200 cm^{-1} correspond to the hydroxyl (O-H) stretching vibrations of water molecules. The specific peaks at 3365.7 cm^{-1}, 3380 cm^{-1}, and 3235.2 cm^{-1} indicate the presence of interlayer water, as well as hydroxide groups associated with the LDH structure. These vibrations are characteristic of LDH materials, confirming the presence of water molecules within the interlayer space. The band recorded at 1617.6 cm^{-1} corresponds to the bending vibration of hydroxyl groups, which can be attributed to both the octahedral layers of the LDH structure and the intercalated water molecules. This peak confirms the presence of hydrogen bonding interactions within the interlayer region, which influence the stability and hydration state of the material. A weak but noticeable band at 2191.67 cm^{-1} in the Zn/Al-SO_4 spectrum was attributed to the stretching vibration of SO_4^{2-} groups. This sulfate-related band suggested the incorporation of sulfate anions into the LDH interlayer, either as charge-balancing species or as part of the structural framework. The sulfate bands further appeared in the lower frequency range, with a characteristic peak at 1364.2 cm^{-1}, corresponding to the asymmetric stretching vibration of SO_4^{2-}. In contrast, the Zn/Al-DADPHA spectrum showed additional distinct peaks that confirmed the intercalation of DADPHA molecules. The peaks observed at 1267 cm^{-1}

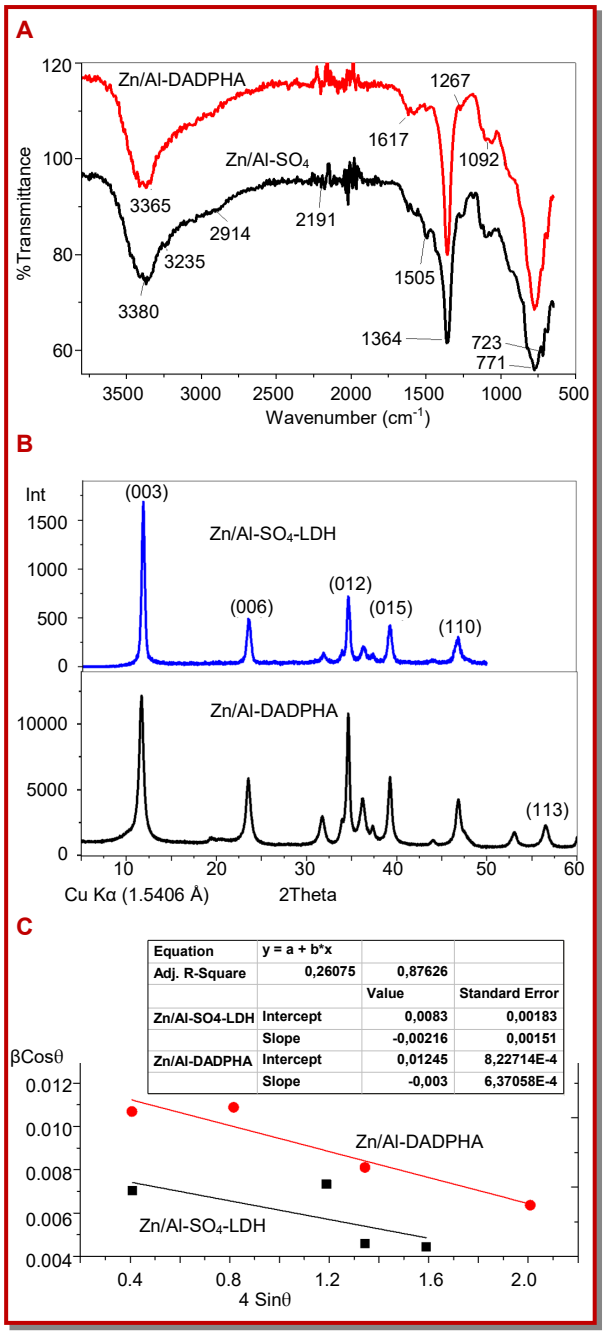

Figure 1: FT-IR spectra (A) and XRD patterns (B) of Zn/Al-SO_4-LDH and Zn/Al-DADPHA. Williamson-Hall plot of βcosθ against 4 sin θ calculated from XRD diffractogram for LDHs

and 1092.1 cm^{-1} correspond to C-N and C-O stretching vibrations, respectively, suggesting the presence of organic functional groups from the DADPHA molecules. These peaks were absent in the Zn/Al-SO4 spectrum, indicating a successful modification of the LDH structure. At lower wavenumbers, the bands around 771.5 cm^{-1} and 723.1 cm^{-1} corresponded to metal -oxygen vibrations, which were characteristic of LDH structures. These peaks arose due to Zn-O, Al-O, and O-M-O bond vibrations, confirming the layered nature of the material.

X-ray diffraction (XRD) analysis

The XRD patterns of both materials, Zn/Al-SO4-LDH and Zn/Al-DADPHA, are depicted in Figure 1B. The synthesized materials exhibited diffraction peaks at various angles 2θ = 11.6°, 23.5°, 34.6°, 39.2°, 46.8°, and 56.5°, corresponding to the basal planes (hkl) of (003), (006), (012), (015), (110), and (113), respectively. The reported crystallographic plane indices demonstrate the successful geometric arrangement and crystalline phases of the prepared LDH materials. However, the Zn/Al-DADPHA material displayed an additional peak at 2θ = 60.2°, which is assigned to the basal plane of (113). The observed peak could be explained by the intercalation of DADPHA onto the LDH material.

Other parameters are extracted from XRD data, such as basal spacing and interlayer space. They were found to be 7.5 and 1.5 angstrom for Zn/Al-SO_4-LDH, and 7.9 and 1.5 angstrom for Zn/Al-DADPHA, respectively. According to JCPDS Card No. 48–1023, the synthesized LDH materials were indexed to a hexagonal structure with the unit cell dimension of a = 3.4 angstrom, c = 21.92 angstrom, and unit cell volume of 216.5 $angstrom^3$.

Furthermore, crystallite size (D) is a critical parameter referring to the size of the individual crystallite of the material. This parameter is inversely related to the full width at half maximum (FWHM) of the X-ray diffraction peak. Based on the Williamson-Hall method, the crystallite sizes of Zn/Al-SO_4 LDH and Zn/Al-DADPHA were computed using the following W-H formula:

$$\beta_T \operatorname{Cos}\theta = \varepsilon(4\operatorname{Sin}\theta) + \left(\frac{K\lambda}{D}\right)$$

D denotes the crystallite size; K represents the Scherrer constant equal to 0.9. λ is the wavelength of the X-ray (in nanometers and equal to 0.15406 nm for CuKα); β designs the full width at half maximum (FWHM) of the diffraction peak (in radians); θ is the Bragg angle

The linear fit of the Williamson-Hall plot is displayed in Figure 1C. The values of the crystallite size of Zn/Al-SO_4-LDH and Zn/Al-DADPHA were determined from the intercept of (Kλ/D), which was found to be 16.7 nm and 11.1 nm, respectively. The corresponding values of Zn/Al-SO_4 LDH and Zn/Al-DADPHA materials were estimated to be 3.6 and 8.1, respectively.

Overall, the XRD analysis confirms the hexagonal layered structure of both materials, while the additional peak and structural variations observed for Zn/Al-DADPHA suggest a successful intercalation of DADPHA molecules, impacting the crystallite size and dislocation density.

Morphological analysis (SEM)

Figure 2 presents the SEM images of the synthesized LDH materials. The micrographs reveal a significant morphological change in Zn/Al-SO_4-LDH before and after intercalation with the phosphonic acid (DADPHA).

The morphology of Zn/Al-SO_4-LDH clearly shows the presence of lamellar particles with a hexagonal layer structure, which is a typical characteristic of hydrotalcite-like materials. The LDH crystals exhibited a well-defined hexagonal platelet-like morphology with numerous microcrystalline platelets stacked together in an irregular arrangement. The SEM images indicate that Zn/Al-DADPHA-LDH morphology had undergone a significant transformation after grafting, with the particles appearing more aggregated. The modified LDH shows a more diffuse surface with less distinct edges compared to the unmodified LDH. The increased porosity of the hybrid material suggests enhanced intercalation with phosphonic acid, leading to the formation of larger interlayer spaces and significant surface porosity. This morphological transformation is expected to influence the physicochemical behavior of the material, potentially enhancing its surface reactivity and adsorption properties.

Antibacterial activity

The antibacterial efficacy of the synthesized novel hybrid material Zn-Al-DADDPHA compound was systematically evaluated against various bacterial strains, revealing distinct inhibition patterns (Table I). While Zn/Al-SO_4 LDH exhibited higher potency overall, Zn/Al-DADDPHA demonstrated significant activity against key pathogens, indicating its potential as an antimicrobial agent.

Against *E. coli* (Table I), Zn/Al-DADDPHA exhibited a substantial inhibition zone of 25.6 ± 2.7 mm, confirming its antibacterial potential. Although Zn/Al-SO_4 LDH showed a higher mean inhibition zone of 34.4 ± 0.0 mm with minimal variability, the inhibition demonstrated by Zn/Al-DADDPHA suggests that it remains a promising candidate, particularly with formulation refinements to enhance its stability and efficacy. Zn/Al-DADDPHA displayed a moderate antibacterial effect against *P. aeruginosa*, with an inhibition zone of 10.9 ± 0.7 mm. Although lower than Zn/Al-SO_4 LDH (25.3 ± 0.2 mm), this result is notable given *P. aeruginosa*'s well-documented resistance to antibiotics. The observed

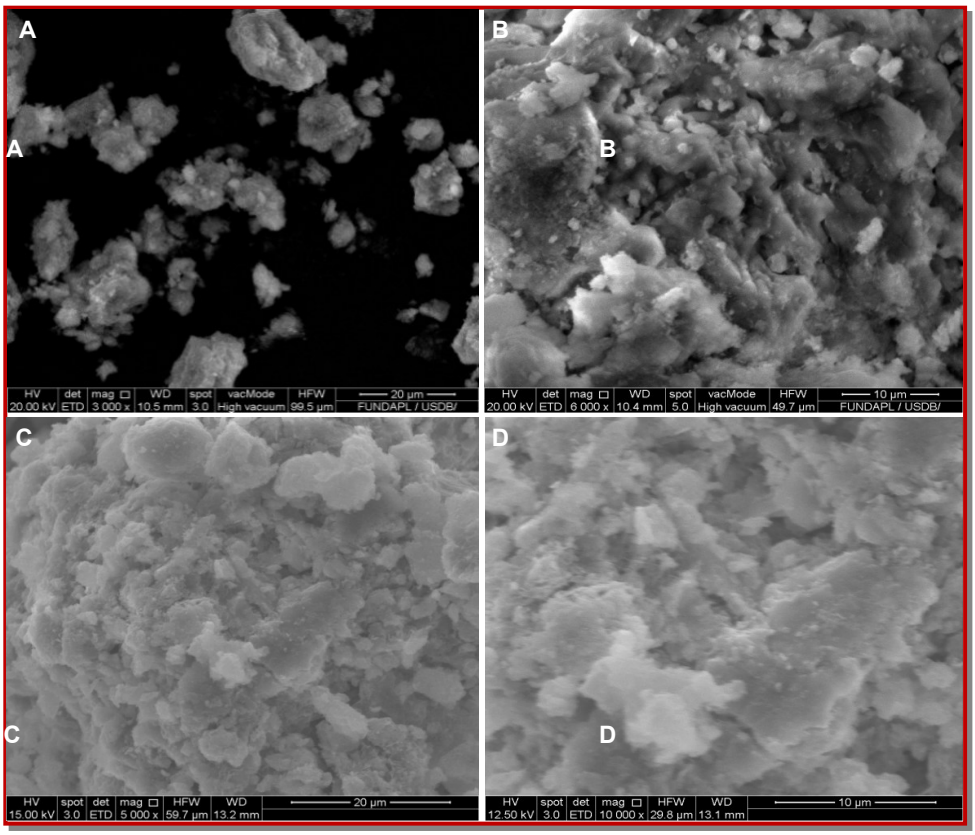

Figure 2: Scanning electron microscope (SEM) micrographs of Zn/Al-SO_4-LDH (A, B) and Zn/Al- DADPHA (C, D)

Table I

Inhibition zones (mm) of synthesized compound against bacterial strains

Bacterial strains	Zn/Al-SO_4 LDH	Zn-Al-DADPHA
E. coli	34.4 ± 0.1	25.6 ± 2.7
P. aeruginosa	25.3 ± 0.3	10.9 ± 0.8
S. aureus	32.2 ± 0.8	30.2 ± 1.5
B. cereus	37.2 ± 1.0	25.5 ± 0.7

Data are mean ± SEM; n=2

activity suggests that Zn/Al-DADPHA may still exert a degree of antimicrobial pressure on this resistant strain, warranting further structural modifications to enhance its performance.

Zn/Al-DADDPHA demonstrated a strong inhibition zone of 30.2 ± 1.5 mm against *S. aureus*, closely approaching the effectiveness of Zn/Al-SO_4 LDH (32.2 ± 0.8 mm). This result highlights Zn/Al-DADPHA as a potent antibacterial agent against Gram-positive bacteria, particularly *S. aureus*, a major pathogen in skin and soft tissue infections. With further optimization, Zn/Al-DADPHA could serve as a valuable antimicrobial component in pharmaceutical and medical applications. Against *B. cereus*, Zn/Al-DADPHA exhibited an inhibition zone of 25.5 ± 0.7 mm, demonstrating considerable antibacterial activity. While Zn/Al-SO_4 LDH achieved a higher inhibition zone (37.2 ± 0.9 mm), the notable efficacy of Zn/Al-DADPHA indicates its potential application in food safety, where *B. cereus* is a major concern due to its role in foodborne illnesses.

Although Zn/Al-SO_4 LDH exhibited consistently stronger inhibition across bacterial strains, Zn-Al-DADPHA showed substantial antimicrobial potential, particularly against Gram-positive bacteria. The observed differences in efficacy suggest that Zn-Al-DADPHA could be further optimized to improve its antibacterial properties, making it a viable candidate for future antimicrobial formulations.

Quantum chemical analysis

The quantum chemical analysis of the ligand DADPHA revealed key electronic properties (Figure 3), including the energies of the HOMO and the LUMO. The HOMO energy was calculated to be -0.38649 eV, and the LUMO energy was 0.10235 eV, giving a HOMO-LUMO gap of 0.48884 eV. This gap suggests moderate reactivity, which may be advantageous for interactions with biological targets. Visualizing the HOMO and LUMO revealed electron-rich regions in the HOMO and electron-deficient regions in the LUMO, providing insights into potential chemical interactions. These findings suggest that DADPHA may form stable, reactive complexes with biological molecules, with potential applications in drug design and molecular

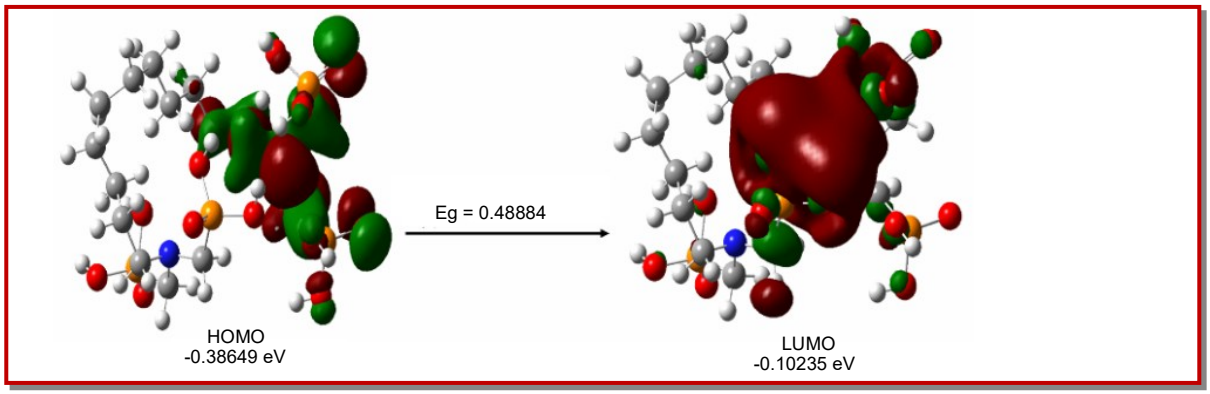

Figure 3: Optimized molecular structures and frontier orbital energy levels of DADPHA

interactions.

Molecular docking analysis

The results presented the binding affinity and molecular interactions of the antimicrobial target proteins with the novel ligand DADPHA. The estimated free energy of binding (ΔG) for the complexes ranges from -6.1 kcal/mol to -5.3 kcal/mol, indicating

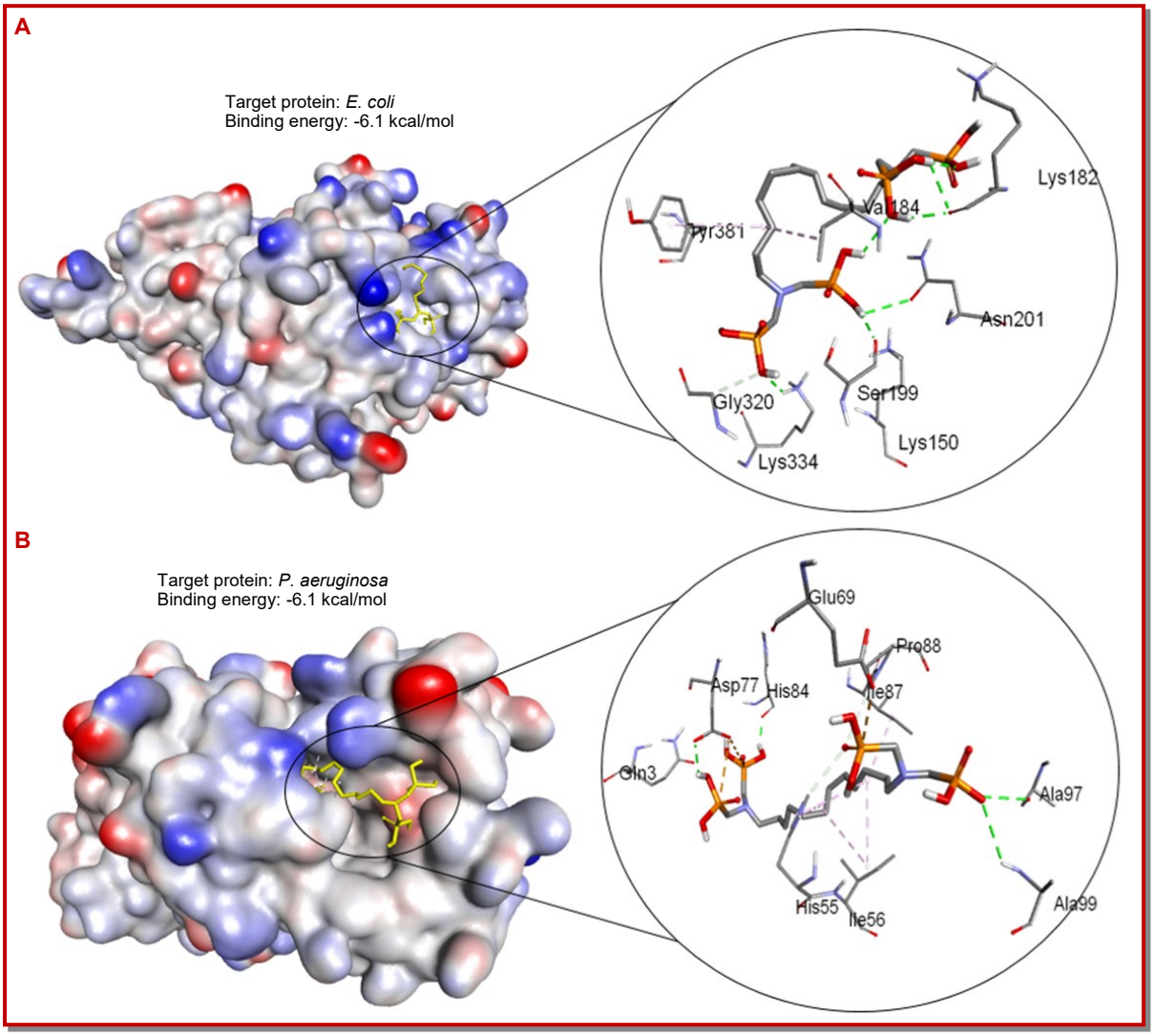

Figure 4: Surface views of the protein-ligand complex (left), enzyme active site, and the 3D structure of enzyme-ligand bonds (inset). The complexes depicted are: 7ONN-DADPHA complex (A), 1YOC-DADPHA complex (B), 7RM7- DADPHA complex (C), 1AH7- DADPHA complex (D). Cont.

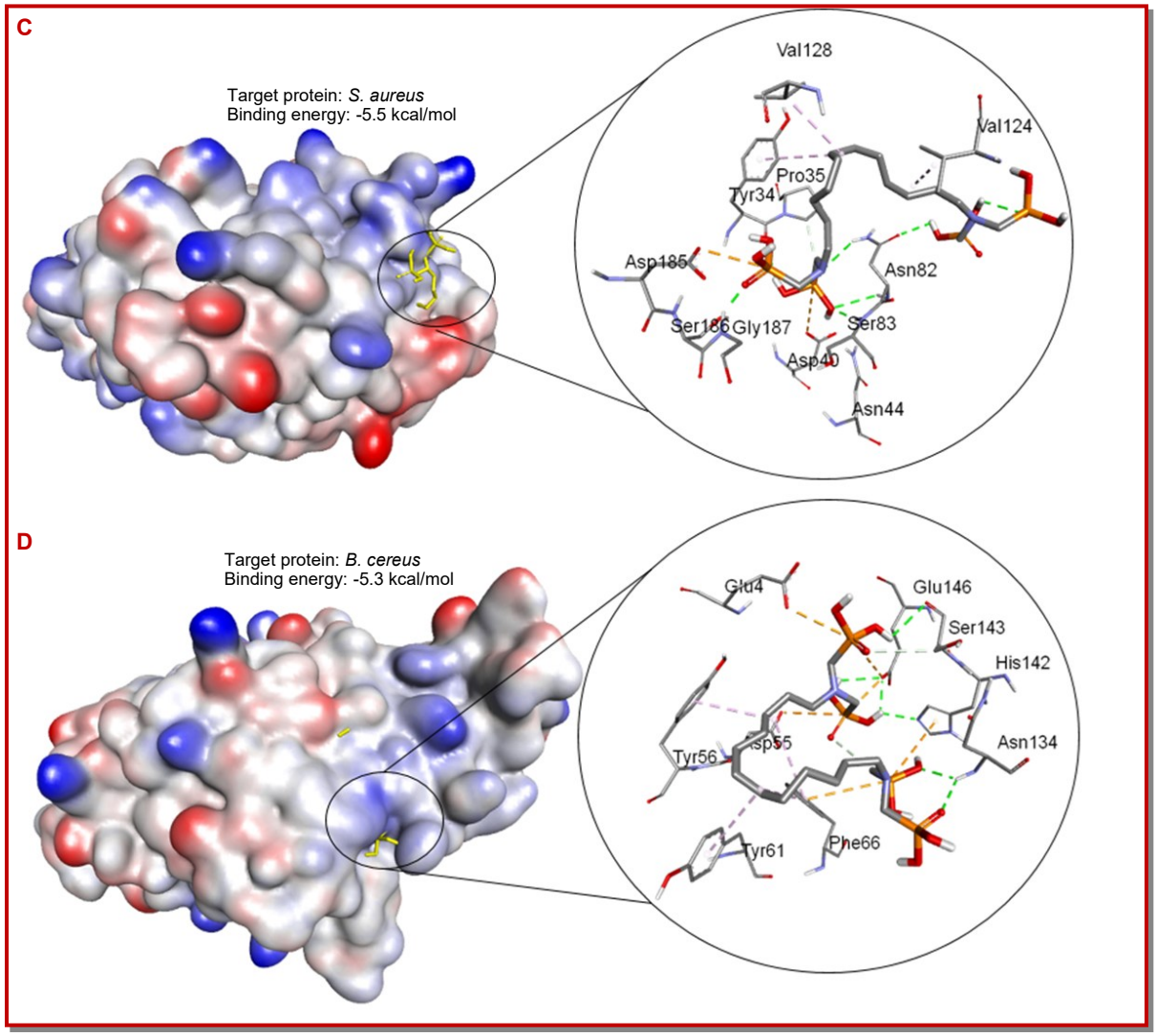

Figure 4: Surface views of the protein-ligand complex (left), enzyme active site, and the 3D structure of enzyme-ligand bonds (inset). The complexes depicted are: 7ONN-DADPHA complex (A), 1YOC-DADPHA complex (B), 7RM7- DADPHA complex (C), 1AH7- DADPHA complex (D)

moderate binding affinity. These values suggest that DADPHA forms stable complexes with target proteins from various bacterial species, including *E. coli*, *P. aeruginosa*, *S. aureus*, and *B. cereus*.

In terms of molecular interactions, the ligand interacts with a range of amino acid residues in the binding pockets of each target protein. For the *E. coli* target protein (PDB ID: 7ONN), DADPHA forms interactions with residues such as Lys150, Lys182, Val184, Ser199, Asn201, Gly320, and Lys334 (Figure 4A). In *P. aeruginosa* (PDB ID: 1YOC), the ligand binds to residues including Gln3, His55, Ile56, Glu69, Asp77, His84, Thr87, Pro88, Ala97, and Ala99 demonstrating a variety of polar and hydrophobic interactions (Figure 4B). The *S. aureus* target protein (PDB ID: 7RM7) shows interactions with residues like Tyr34, Pro35, Asp40, Asn44, Asn82, Ser83, Val124, Val128, Asp185, Ser186, and Gly187 which could suggest a mix of hydrogen bonding and van der Waals interactions (Figure 4C). Lastly, for the *B. cereus* target protein (PDB ID: 1AH7), the interactions involve Glu4, Tyr56, Tyr61, Phe66, Asn134, His142, Ser143, and Glu146, which are likely critical for the stability and specificity of the binding (Figure 4D).

These interactions highlight the versatility of DADPHA in engaging with different target proteins across bacterial species, potentially explaining its broad-spectrum antimicrobial potential. The consistent binding affinity across these targets suggests that DADPHA could be an effective antimicrobial agent, with the specific residues involved in binding offering insight into the molecular mechanisms of interaction.

Molecular dynamics analysis

The RMSD values, as depicted in Figure 5A, indicated significant variability among the complexes studied.

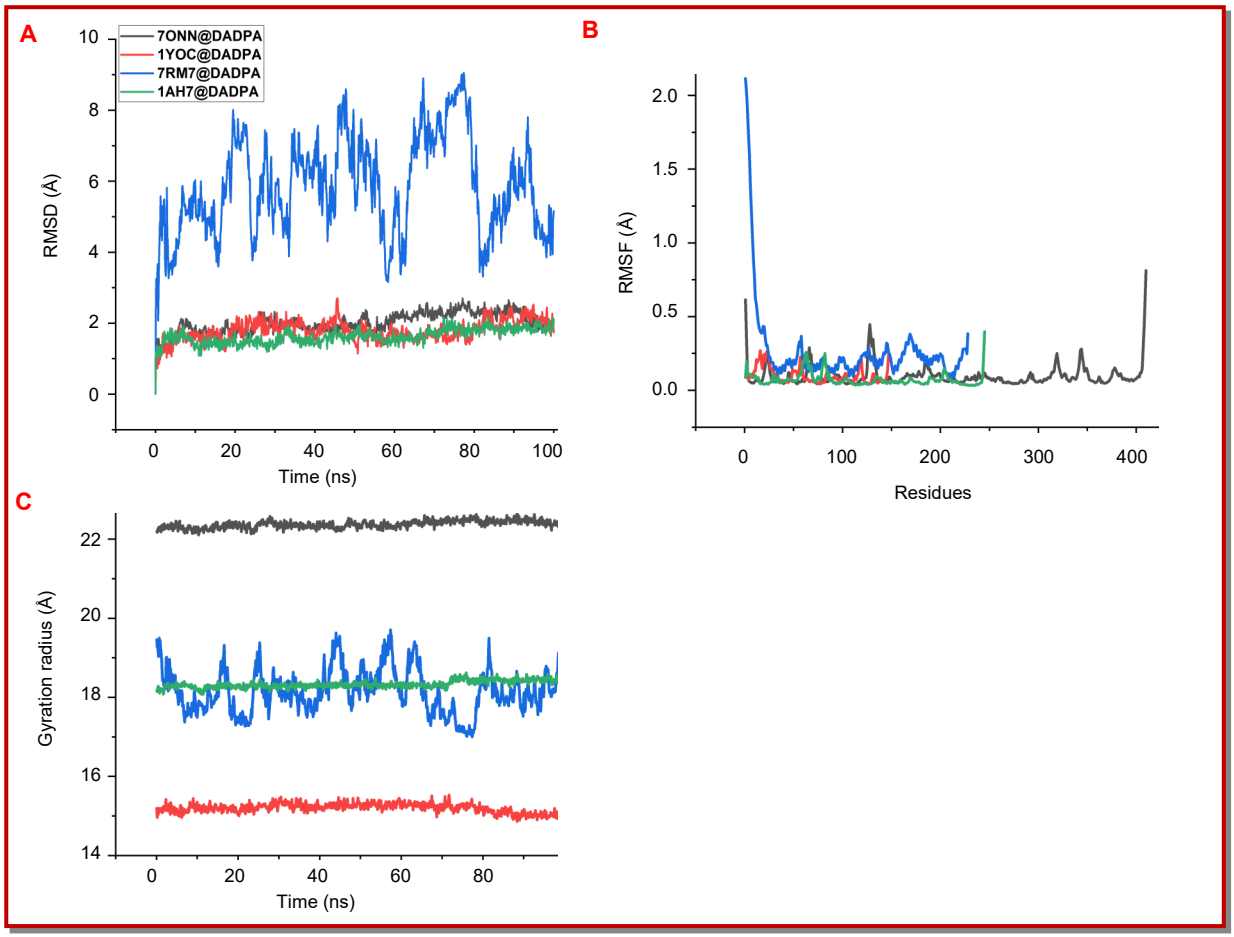

Figure 5: Molecular dynamic analysis of the target proteins complexed with DADDPHA. Root mean square deviation (RMSD) (A), root mean square fluctuation (RMSF) (B), and radius of gyration (Rg) trajectories (C)

The 7RM7@ DADDPHA complex demonstrated the highest RMSD fluctuations, ranging between 4 and 8 angstrom, suggesting considerable conformational changes and potential instability. In contrast, the 1YOC@ DADDPHA and 7ONN@ DADDPHA complexes maintained RMSD values below 2 angstrom, indicating their structural stability. The observed stability of the 1YOC and 7ONN complexes suggests a stabilizing effect of ligand binding, whereas the increased flexibility of 7RM7 implies possible structural perturbations induced by ligand interaction. As shown in Figure 5B, most residues exhibited fluctuations below 0.5 angstrom, indicating limited flexibility and suggesting structural rigidity of the protein-ligand interactions. However, the N- and C-terminal regions displayed relatively higher fluctuations, a typical behavior in proteins. The 7RM7@ DADDPHA complex showed slightly higher fluctuations in specific regions, implying localized conformational changes that may impact ligand binding stability. Conversely, the lower RMSF values observed in the 1YOC@ DADDPHA and 7ONN@ DADDPHA complexes indicated a stabilizing influence of the ligand, reinforcing protein rigidity and reducing local flexibility. The Rg values, illustrated in Figure 5C, revealed notable differences in the structural compactness of the studied complexes. The 1YOC@ DADDPHA complex exhibited the lowest Rg values (~14–16 angstrom), indicative of a well-folded and stable structure. The 7ONN@ DADDPHA complex (black) showed the highest Rg values (~22–24 angstrom), suggesting a more expanded conformation, which might reflect potential destabilization or ligand-induced structural changes. The 7RM7@ DADDPHA and 7ONN@ DADDPHA complexes displayed moderate compactness with Rg values fluctuating around 17–19 angstrom.

Discussion

This study synthesized and characterized a novel Zn/Al-diaminododecylphosphonic acid layered double hydroxide and evaluated its structural, electronic, and antibacterial properties. FT-IR spectroscopy confirmed the presence of functional groups crucial for the observed biological and physicochemical properties. The broad O-H stretching band at ~3300 cm^{-1} indicates strong hydrogen bonding, which plays a key role in enhancing antimicrobial activity by disrupting bacterial

membranes (Si et al., 2021). Additionally, the presence of C=O stretching at ~1700 cm^{-1} corresponds to carbonyl functionalities, which are known to facilitate metal coordination in biomaterials (Al-Fakeh et al., 2023). These functionalities contribute to bioactivity by forming hydrogen bonds with bacterial cell wall components, leading to cell membrane destabilization (Nassarawa et al., 2023). XRD analysis revealed distinct diffraction peaks, indicating a semi-crystalline nature. The degree of crystallinity affects both solubility and interaction with bacterial cell walls, influencing antimicrobial efficacy. Crystalline phases have been reported to enhance surface reactivity, allowing effective bacterial adhesion disruption (Kumar and Engle, 2023). Additionally, the presence of sharp peaks in the diffractogram confirms the ordered arrangement of molecules, which can modulate electron transfer mechanisms during quantum chemical interactions (Wang et al., 2023). SEM analysis images showed a rough and porous surface morphology. The rough texture increases surface area, thereby promoting better interaction with microbial membranes. This observation aligns with studies where porous nanomaterials exhibited enhanced antibacterial efficacy due to mechanical cell wall disruption (Rezaei et al., 2024). The microstructural features observed also suggest strong electrostatic interactions between the material and negatively charged bacterial membranes, leading to cell membrane damage and leakage of cytoplasmic content (Roy et al., 2022). In addition, the antimicrobial efficacy observed can be attributed to multiple mechanisms, including oxidative stress induction, membrane disruption, and metabolic enzyme inhibition. The presence of hydroxyl (-OH) and carbonyl (-C=O) groups facilitates reactive oxygen species (ROS) generation, leading to oxidative stress in bacterial cells (Zhang et al., 2023). Similarly, electrostatic interactions between negatively charged bacterial membranes and positively charged surface functionalities promote membrane destabilization (Vejzovic et al., 2022). Recent studies highlight that such interactions result in increased permeability, leakage of essential biomolecules, and eventual bacterial cell death (Modi et al., 2023). Regarding quantum chemical calculations, DFT analysis provided insights into electronic structure, charge distribution, and reactivity. The highest HOMO and LUMO energy gap (ΔE) influences electron transfer capabilities, impacting interactions with biomolecules (Almeida et al., 2017). A low ΔE value suggests enhanced reactivity, facilitating redox reactions that contribute to antimicrobial effects (Ebrahimian et al., 2022). Additionally, electrostatic potential mapping indicated regions of high electron density, which play a crucial role in hydrogen bonding with bacterial components, further strengthening the observed bioactivity (Sultana et al., 2024).

Finally, molecular docking revealed that DADPHA interacts with key bacterial target proteins through hydrogen bonding and hydrophobic interactions, with binding affinities ranging from -6.1 to -5.3 kcal/mol. Stronger binding to *E. coli* (7ONN) and *P. aeruginosa* (1YOC) suggests higher inhibitory potential, likely due to favorable electrostatic and steric interactions (Almalki et al., 2022). These interactions may interfere with enzymatic activity, disrupting bacterial function (Donadio et al., 2021). Molecular dynamics simulations confirmed the stability of the complexes, with *P. aeruginosa* and *E. coli* showing RMSD values below 2 angstrom, indicating minimal structural fluctuations. In contrast, *S. aureus* (7RM7) exhibited higher RMSD (4–8 angstrom), suggesting conformational changes that may affect ligand retention (Liu and Kokubo, 2017). The radius of gyration (Rg) analysis further supported the compact stability of *P. aeruginosa,* while *E. coli* showed a more flexible conformation (Manzoor et al. 2021).

Despite the promising results, this study has certain limitations. First, the antibacterial activity was assessed using in vitro methods, and further in vivo studies are required to confirm its efficacy in biological systems. Second, while molecular docking and MD simulations provided insights into ligand-protein interactions, experimental validation of binding mechanisms, such as isothermal titration calorimetry (ITC) or surface plasmon resonance (SPR), was not performed. Additionally, the synthesized Zn/Al-DADPHA LDH material requires further cytotoxicity and biocompatibility assessments before potential biomedical applications can be considered. Finally, the electronic properties were evaluated using DFT calculations, but additional experimental techniques, such as UV-Vis spectroscopy and electrochemical studies, would enhance the understanding of its electronic behavior.

Conclusion

Zn/Al-DADPHA-LDH was successfully synthesized and characterized, confirming its structural integrity through XRD, FTIR, and SEM analyses. Antibacterial assays demonstrated significant inhibitory effects against both Gram-positive and Gram-negative bacteria. Molecular docking and DFT analyses revealed robust binding interactions between DADPHA and bacterial target proteins. Additionally, MD simulations validated the stability of the ligand-protein interactions, further supporting its potential for biomedical applications.

Financial Support

Self-funded

Ethical Issue

Not applicable

Conflict of Interest

The authors declare no conflict of interest.

References

Al-Fakeh MS, Alazmi MS, El-Ghoul Y. Preparation and characterization of nano-sized CO (II), CU (II), MN (II) and NI (II) coordination PAA/alginate biopolymers and study of their biological and anticancer performance. Crystals. 2023; 13: 1148.

Almalki AJ, Ibrahim TS, Elhady SS, Hegazy WA, Darwish KM. Computational and biological evaluation of β-adreno-receptor blockers as promising bacterial anti-virulence agents. Pharmaceuticals 2022; 15: 110.

Almeida MO, Barros DA, Araujo SC, Faria SH, Maltarollo VG, Honorio KM. Study on molecular structure, spectroscopic properties (FTIR and UV–Vis), NBO, QTAIM, HOMO-LUMO energies and docking studies of 5-fluorouracil, a substance used to treat cancer. Spectrochim Acta Part A Mol Biomol Spectrosc. 2017; 184: 169-76.

Arribat M, Cavelier F, Remond E. Phosphorus-containing amino acids with a P–C bond in the side chain or a P–O, P–S or P–N bond: From synthesis to applications. RSC Adv. 2020; 10: 6678-724.

Cao Y, Zheng D, Zhang F, Pan J, Lin C. Layered double hydroxide (LDH) for multi-functionalized corrosion protection of metals: A review. J Mater Sci Technol. 2022; 102: 232-63.

Chen Q, Yu Y, Li J, Nan H, Luo S, Jia C, Deng P, Zhong S, Tian X. Recent progress in layered double hydroxide-based electrocatalyst for hydrogen evolution reaction. Chem Electro Chem. 2022; 9: e202101387.

Donadio G, Mensitieri F, Santoro V, Parisi V, Bellone ML, De Tommasi N, Izzo V, Dal Piaz F. Interactions with microbial proteins driving the antibacterial activity of flavonoids. Pharmaceutics. 2021; 13: 660.

Dubnova L, Daňhel R, Meinhardova V, Korolova V, Smolakova L, Kondratowicz T, Kikhtyanin O, Capek L. Reconstruction of the ZnAl mixed oxides into the layered double hydroxide catalysts active in the aldol condensation of furfural: The role of ZnO particles. Front Chem. 2022; 9: 803764.

Ebrahimian J, Khayatkashani M, Soltani N, Yousif QA, Salavati-Niasari M. Catechin mediated green synthesis of Au nanoparticles: Experimental and theoretical approaches to the determination HOMO-LUMO energy gap and reactivity indexes for the (+)-epicatechin (2S, 3S). Arabian J Chem. 2022; 15: 103758.

Jiang W, Faid AY, Gomes BF, Galkina I, Xia L, Lobo CMS, Desmau M, Borowski P, Hartmann H, Maljusch A. Composition-dependent morphology, structure, and catalytical performance of nickel–iron layered double hydroxide as highly-efficient and stable anode catalyst in anion exchange membrane water electrolysis. Adv Funct Mater. 2022; 32: 2203520.

Kaboudin B, Daliri P, Faghih S, Esfandiari H. Hydroxy-and amino-phosphonates and bisphosphonates: Synthetic methods and their biological applications. Front Chem. 2022; 10: 890696.

Kadari M, Kaid Mh, Ben Ali M, Villemin D. The intercalation of Zn/Al-HDL by the diamino-dodecylphosphonic acid: Synthesis and properties of adsorption of basic fuchsine. J Chinese Adv Mater Soc. 2016; 4: 148-57.

Kim TH, Lee GJ, Kang JH, Kim HJ, Kim Ti, Oh JM. Anticancer drug-incorporated layered double hydroxide nanohybrids and their enhanced anticancer therapeutic efficacy in combination cancer treatment. Biomed Res Int. 2014; 2014: 193401.

Kumar G, Engle K. Natural products acting against *S. aureus* through membrane and cell wall disruption. Nat Prod Rep. 2023; 40: 1608-46.

Liu K, Kokubo H. Exploring the stability of ligand binding modes to proteins by molecular dynamics simulations: A cross-docking study. J Chem Inf Model. 2017; 57: 2514-22.

Liu X, Wu Y, Zhao X, Wang Z. Fabrication and applications of bioactive chitosan-based organic-inorganic hybrid materials: A review. Carbohydr Polym. 2021; 267: 118179.

Mallakpour S, Radfar Z, Hussain CM. Current advances on polymer-layered double hydroxides/metal oxides nano-composites and bionanocomposites: Fabrications and applications in the textile industry and nanofibers. Appl Clay Sci. 2021; 206: 106054.

Manzoor S, Ahmed A, Moin ST. Iron coordination to pyochelin siderophore influences dynamics of FptA receptor from *Pseudomonas aeruginosa*: A molecular dynamics simulation study. Biometals. 2021; 34: 1099-119.

Mishra G, Dash B, Pandey S, Mohanty PP. Antibacterial actions of silver nanoparticles incorporated Zn–Al layered double hydroxide and its spinel. J Environ Chem Eng. 2013; 1: 1124-30.

Miyata S. The syntheses of hydrotalcite-like compounds and their structures and physico-chemical properties—I: The systems Mg^{2+}-Al^{3+}-NO^{3-}, Mg^{2+}-Al^{3+}-Cl^{-}, Mg^{2+}-Al^{3+}-ClO^{4-}, Ni^{2+}-Al^{3+}-Cl^{-} and Zn^{2+}-Al^{3+}-Cl^{-}. Clays Clay Miner. 1975; 23: 369-75.

Modi SK, Gaur S, Sengupta M, Singh MS. Mechanistic insights into nanoparticle surface-bacterial membrane interactions in overcoming antibiotic resistance. Front Microbiol. 2023; 14: 1135579.

Nassarawa SS, Nayik GA, Gupta SD, Areche FO, Jagdale YD, Ansari MJ, Hemeg HA, Al-Farga A, Alotaibi SS. Chemical aspects of polyphenol-protein interactions and their antibacterial activity. Crit Rev Food Sci Nutr. 2023; 63: 9482-505.

Nava-Andrade K, Carbajal-Arizaga G, Obregon S, Rodriguez-Gonzalez V. Layered double hydroxides and related hybrid materials for removal of pharmaceutical pollutants from water. J Environ Manage. 2021; 288: 112399.

Obalova L, Karaskova K, Jiratova K, Kovanda F. Effect of potassium in calcined Co–Mn–Al layered double hydroxide on the catalytic decomposition of N_2O. Appl Catal B

Environ. 2009; 90: 132-40.

Ouazene M, Kaid Mh, Ilikti H, Villemin D. Solvent extraction of samarium (III) by diaminododecylphosphonic acid followed by UV/Vis spectroscopy using arsenazo III. Phys Chem Liquids. 2016; 54: 552-62.

Rashad MM, El-Sayed IE, Galhoum AA, Abdeen MM, Mira HI, Elshehy EA, Zhang S, Lu X, Xin J, Guibal E. Synthesis of α-aminophosphonate based sorbents–Influence of inserted groups (carboxylic vs. amine) on uranyl sorption. Chem Eng J. 2021; 421: 127830.

Rezaei FY, Pircheraghi G, Nikbin VS. Antibacterial activity, cell wall damage, and cytotoxicity of zinc oxide nanospheres, nanorods, and nanoflowers. ACS Appl Nano Mater. 2024; 7: 15242-54.

Roy S, Sarkhel S, Bisht D, Hanumantharao SN, Rao S, Jaiswal A. Antimicrobial mechanisms of biomaterials: From macro to nano. Biomater Sci. 2022; 10: 4392-423.

Saidin S, Jumat MA, Amin NAA, Al-Hammadi ASS. Organic and inorganic antibacterial approaches in combating bacterial infection for biomedical application. Mater Sci Eng C. 2021; 118: 111382.

Sharma A, Kumari S, Sharma S, Singh T, Kumar S, Thakur A, Bhatia S, Sharma A. Layered double hydroxides: An insight into the role of hydrotalcite-type anionic clays in energy and environmental applications with current progress and recent prospects. Mater Today Sustain. 2023; 22: 100399.

Shirin VA, Sankar R, Johnson AP, Gangadharappa H, Pramod K. Advanced drug delivery applications of layered double hydroxide. J Control Release. 2021; 330: 398-426.

Si Z, Hou Z, Vikhe YS, Thappeta KRV, Marimuthu K, De PP, Ng OT, Li P, Zhu Y, Pethe K. Antimicrobial effect of a novel chitosan derivative and its synergistic effect with antibiotics. ACS Appl Mater Interfaces. 2021; 13: 3237-45.

Soleymani M, Kabirifard H, Hekmati M, Esmaeili A, Veisi H. *In situ* bio-inspired fabrication of Ag nanoparticles on *Matricaria chamomilla* extract modified Cu-Al-Zn LDH as a beneficial antimicrobial agent. Inorg Chem Commun. 2024; 160: 111998.

Stamate AE, Pavel OD, Zavoianu R, Birjega R, Neubauer K, Koeckritz A, Marcu IC. Study of the catalytic properties of MgNi (Cu) Al LDH in the one-pot cascade oxidation-Knoevenagel condensation reaction. Mol Catal. 2023; 537: 112968.

Sultana S, Hossain MA, Biswas S, Saleh MA, Ali F, Kawsar SM. Chemical reactivity, molecular electrostatic potential, FTIR, NMR, *in vitro*, and *in silico* studies of mannopyranoside derivatives: 3-Nitrobenzoylation leads to improve antimicrobial activity. Chem Phys Impact. 2024; 9: 100692.

Theiss FL, Ayoko GA, Frost RL. Synthesis of layered double hydroxides containing Mg^{2+}, Zn^{2+}, Ca^{2+} and Al^{3+} layer cations by co-precipitation methods: A review. Appl Surf Sci. 2016; 383: 200-13.

Vejzovic D, Piller P, Cordfunke RA, Drijfhout JW, Eisenberg T, Lohner K, Malanovic N. Where electrostatics matter: Bacterial surface neutralization and membrane disruption by antimicrobial peptides SAAP-148 and OP-145. Biomolecules 2022; 12: 1252.

Wang M, Chen Y, Yu Z, Hou Y, Jiang R, Li S, Chen J, Tang W, Pang H, Xie W. Unraveling the π-interaction of NiFe-based metal–organic frameworks with enhanced oxygen evolution: Optimizing electronic structure and facilitating electron transfer modulation. J Colloid Interface Sci. 2023; 640: 1-14.

Wei C, Yan X, Zhou Y, Xu W, Gan Y, Zhang Y, Zhang N. Morphological control of layered double hydroxides prepared by co-precipitation method. Crystals 2022; 12: 1713.

Zavoianu R, Mihaila SD, Cojocaru B, Tudorache M, Parvulescu VI, Pavel OD, Oikonomopoulos S, Jacobsen EE. An advanced approach for MgZnAl-LDH catalysts synthesis used in Claisen-Schmidt condensation. Catalysts 2022; 12: 759.

Zhang J, Su P, Chen H, Qiao M, Yang B, Zhao X. Impact of reactive oxygen species on cell activity and structural integrity of Gram-positive and Gram-negative bacteria in electrochemical disinfection system. Chem Eng J. 2023; 451: 138879.

Author Info

Djamila Ikhou and M'hamed Kaid (Principal contact)
e-mail: djamilaikhou77@gmail.com and kaidmhamed@yahoo.fr